Fatigue Fracture of AZ91 Magnesium Alloy

[1]Subash Chandrabose E, [2]Gokulakrishnan M, [3]Naveenkumar P and [4]Babu C
[1,2,3,4] Department of Mechanical Engineering, Sri Eshwar College of Engineering, Coimbatore, Tamil Nadu, India.
[1]subashchandrabose.e2019mech@sece.ac.in, [2]gokulakrishnan30062002@gmail.com, [3]naveen2832002@gmail.com, [4]babu.cmech@sece.ac.in

Article Info
S. Venkatesh et al. (eds.), *1st International Conference on Emerging Trends in Mechanical Sciences for Sustainable Technologies,* Advances in Computational Intelligence in Materials Science.
Doi: https://doi.org/10.53759/acims/978-9914-9946-6-7_6

Abstract - On today's environment, the use of the proper material is critical in every business. Materials must be suitable for or meet the specifications of the industrial component. Magnesium alloys are well recognized as the lightest structural alloys. To strengthen its physical attributes, mg is alloyed with other elements. Mn, Al, silicon, Zn, Cu, zircon, and rare-earth metals are among these elements. Various levels of provokes can be seen according to the chemical composition. So, while adding new alloying elements to the material, it will be move to research and the end results will be compared with the previous material. Fracture toughness is the science of understanding the failure of materials with cracks and defects. Fracture mechanics is used to calculate the anxiety levels at which cracks of a specified size can migrate through the material and cause failure. As the Mg alloy material has been introduced to replace the aluminium and also it should carry steel materials in the field of manufacturing the electric vehicles. The Electric vehicle requires very light weight materials and also it should carry out the load more efficiently. To find the actual capacity of the metal workpiece the (AZ91) mg alloy has been purchased. After purchasing the material, the metal has been cut as per the (ASTM) standards with the desired dimensions. When the metal cutting has completed, the metal is given to the heat treatment process to increase its strength. After all these processes, the material is given to the laboratory to know the fracture studies of the metal, the results are presented in result and discussion section.

Keywords - ASTM Standard, AZ91 Alloy, Applications.

I. INTRODUCTION

Joseph Black established the magnesium in the year 1755. The word "Magnesia," which refers to a region on the east side of Thessaly in Greece, is where the metal "Magnesium" first got its name. This magnesium is the ninth liberal metal to be found in the crust of the earth. The crust of the planet contains up to 2% magnesium alloys. And for small applications, mg alloys are typically preferred. In order to create a new material and boost the material's physical strength, magnesium is added to other materials to create magnesium alloys. This is how those alloys are created. These magnesium alloys are biodegradable by nature and have an elasticity that is similar to that of human bones (approximately 45GPa). Magnesium alloys are useful for decadence in their natural environment since they are nano-structured and connected to human bodies in terms of metabolic interactions. The ability to select any material to make a design more effective plays a crucial role in all aspects of design, which is why this magnesium alloy was selected. Despite the magnesium alloys' great strength and light weight, there are some restrictions in the way the material is designed. These restrictions determine the material's inherent fragile at ambient condition, which is connected in an arrangement such that semestral neighbouring cram crystals. Pure magnesium alloys have these kinds of restrictions, but they can be improved by incorporating new key metal segments to make new magnesium alloys with improved qualities and to get more benefits. Due to this, more studies have been conducted on mg alloys to discover novel alloy types and employ them in various categories based on their qualities.

II. II. AZ91 MAGNESIUM ALLOY

The most popular die casting magnesium alloy is AZ91, which combines castability, corrosion resistance, and mechanical strength qualities. Magnesium's restriction of slip systems prevents substantial deformation due to its spheres packed by the alternate layers structure, which limits its deformability and requires work strengthening. The main challenges in AZ91 magnesium alloy are the cereal confines. As a result, the composite adheres to the Hall-Petch relationship. When magnesium alloys fail, brittle fracture is typically assumed, and the most frequent fracture modes are cleavage and quasi-cleavage [1]. Magnesium typically cleaves along the crystal plane 0001. The Mg Al phase is the primary strengthening intermetallic for AZ91 magnesium alloy. The magnesium matrix's its structure is incompatible with the cubic primitive Mg Al formation, which results in the MgrMg Al interface's fragility. Additionally, Mg Al it 17 12 17 12 w x self is weak and rather soft 6. Micro cracks frequently start at the MgrMg Al attachment and even in Mg Al 17 12 17 12 particles as a result. The mechanical characteristics of the AZ91 alloy are significantly influenced by the

volume and shape of Mg Al 17 12. Modern estimate methodologies for cleavage manner, including breakage, quasi-breakage, microscopic void fusion, etc., are depending on the study of ferrous mixture and may not be appropriate for non-ferrous metals, particularly hexagonal closed pack magnesium alloy [2]. Magnesium alloy splintering exterior configuration can be easily changed by changing alloying components and experimental conditions. Nevertheless, nothing is now known regarding the cleavage behaviour of mg alloys. The current work examined the tensile and impact test fracture behaviour of the AZ91 alloy [3].

III. III. METAL CUTTING

ASTM E647

The material, chemical, mechanical, and metallurgical properties of metals must be assessed using ASTM standards shown in **Fig 1**. The product producers can use this information to help them choose the right application and processing techniques. More than 12,000 standards in every area are searchable on the ASTM website by organizations and individuals.

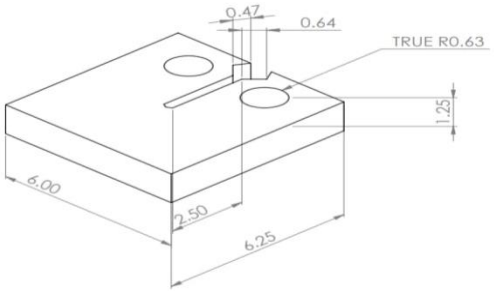

Fig 1. Design of Work Specimen.

WEDM (wire electrical discharge machining) process

According to their towering robustness to load ratio and required physical qualities, magnesium alloys find extensive use in the aircraft and self-propelling production. In the current study, the effects of three WEDM process input specification such as pulse on time, servo feed rate, and pulse current were examined in relation to the performance metrics of metal shifting outlay, indentation breadth, and aspect asperity when milling the magnesium alloy AZ91[4]. This study, which is the first in-depth investigation of magnesium alloys subjected to electrical discharge machining, examines the formability and behaviour of materials with less liquefy points and towering thermal conductivities under this process. The percentage contribution of each variable input framework on output framework was calculated using the reciprocation aspect modus operandi [5]. The outcome of the survey of variance manifest that, while the servo feed rate had a negligible impact on the process output parameters, pulse current and pulse on time did. The speculative outcome demonstrated that the metal shifting outlay and indentation spread during the wire cutting process of magnesium is significantly surpassing that of hard materials, and can reach up to 160 mm 6 min 3, while the kerf spread and metal side face roughness are approximately 0.400 and 4.783 m, respectively. High machinability of mg mixture by this wire cutting process is indicated by the aspect roughness being suitable and also comparable to hard materials despite the high cutting rate [6][7]. EDX survey, SEM, and fissionable energy microscopy have all been waged to analyse the surface topography and microstructural alterations. SEM micro graphs reveal that there are few micro cracks, which are signs of surface damage, on the machined surface, demonstrating WEDM's capacity to create work surfaces without damage. The maximum and minimum recast layer thicknesses are 3.09 and 6.91 mm, respectively.

IV. COMPACT TENSION SPECIMEN

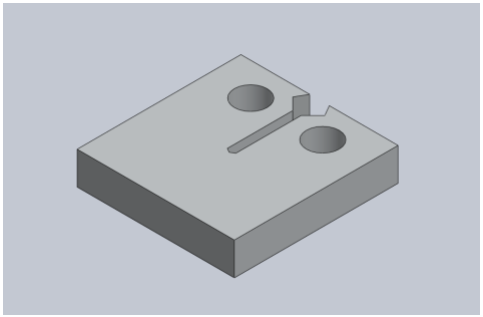

Fig 2. work Specimen.

In this study, the AZ91 Mg alloy plate notched compact tension specimens with stress applied in both the rolling direction (RD) and transverse direction are used for Mode-I fracture studies (TD) shown in **Fig 2**. Both RD and TD

specimens exhibit moderately high JC 46 N/mm notched fracture toughness [8]. Crack tunnelling is visible on the fracture face at the sample piece midpoint and there are several shear mouths close to the free surface. SEM fractographs show dimples, which suggests ductile fracture. ahead of the cleft in the connective, EBSD examination reveals extensive tensile twinning. The toughness of the notched fracture specimens with reduced triaxiality is demonstrated to be enhanced by tensile twinning in two different ways. It adds hardening to the background plastic zone and offers significant dissipation. It has been demonstrated that tensile twinning has two effects on the toughness of specimens with notched fractures but diminished triaxiality. By operating a number of mechanisms, it offers significant dissipation in the background plastic area and imparts hardening to the material around the fracture process area, Postponing the development and coarsening of segments and sub.

V. CRYOGENIC TREATMENT

The cryogenic procedure involved gradually lowering the temperature of the specimens to 88 K at a rate of 2 K per minute, maintaining this less degree for a predetermined amount of time, and then gradually bringing the specimens back up to room temperature which is shown in the results in **Fig 3**. A well insulated treatment room with liquid N serving as the working fluid was used to attain the extremely low temperature. For 2, 4, 24, and 48 hours, the influence of the soaking time parameter was examined [9][10]. The cryogenic treatment is a test which will be done in the level of minus subzero level of treatment, when in Shallow treatment the work will be done for 24 hrs the degree level will be upto (-86) degree celcius for the work piece specimen. Another type of treatment is Deep in this the degree will decrease upto (-190) degree celcius the work will be done upto 72 hours [11]. Mg alloys are being utilised more frequently in the electrical, automotive, and aircraft industries thanks to its less thickness, high level unique power, great moistening capabilities, outstanding machine's capacity, and good electromagnetic protecting qualities. Cryogenic test is a procedure which modifies the properties of materials to improve their performance by subjecting them to a cryogenic temperature. An increase in interest in using CT on various materials has been noted over the past few years [12].

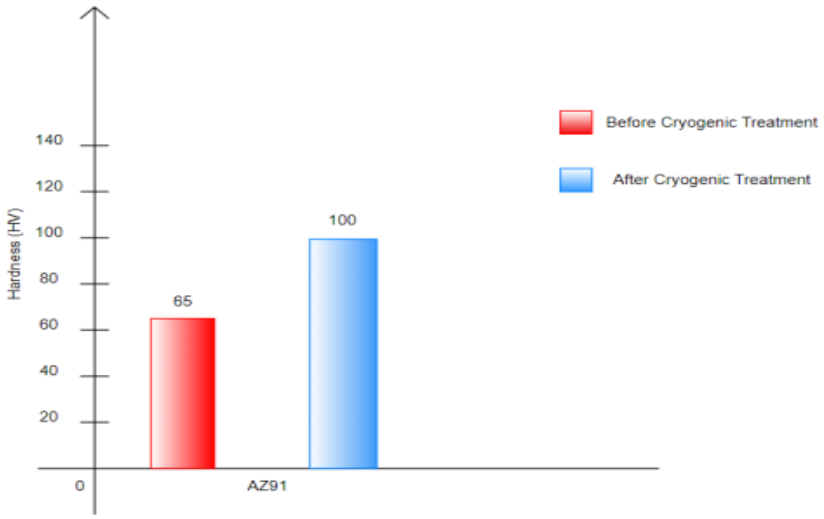

Fig 3. Hardness Test Results.

Tool steels, particularly high-speed steel, have been the focus of the majority of research on Cryogenic Test in the field of machining equipment and cutting equipment's of materials shown in **Table 2**. The effects of this treatment on metals are explained by two key factors. First off, CT can almost entirely turn any remaining austenite into martensite. Second, the precipitation of submicroscopic carbides as a result of the CT can be used to explain the improvement in mechanical properties [13]. A number of aeronautical, motor sport and semiconductor companies in China, the Us, and other developed nations have incorporated this method into their routine rehabilitation lines to boost fatigue rate and low shrinkage of components. Mechanical properties of mg alloy, on the other hand, have received little attention. The current study focused on the evolution of the morphology, annealing, and tensile and extramural characteristics of AZ91 mg alloy samples during Cryogenic Treatment shown in **Table 1**. The term "cryogenic treatment" refers to the handling of minerals at temperatures between -230°C and 190°C. Since steel's hardness and wear resistance are vastly increased following cryogenic treatment, CT is frequently employed in the fabrication of steel [14]. While just a few studies have been described, the analysis of this test on mg alloy seems to be quite important. Thus, the current study examines how this treatment affects the interracial and mechanical behavior of the alloy AZ91 which is shown in **Fig 4**. This work has presented a unique approach for the study of Mg alloy as it is a systematic investigation of the precipitating behaviour, microstructure evolution, and material strength of Mg alloy under cryogenic treatment. Also, a novel method for Mg alloy has been proposed, which may have substantial ramifications and promising application possibilities [15].

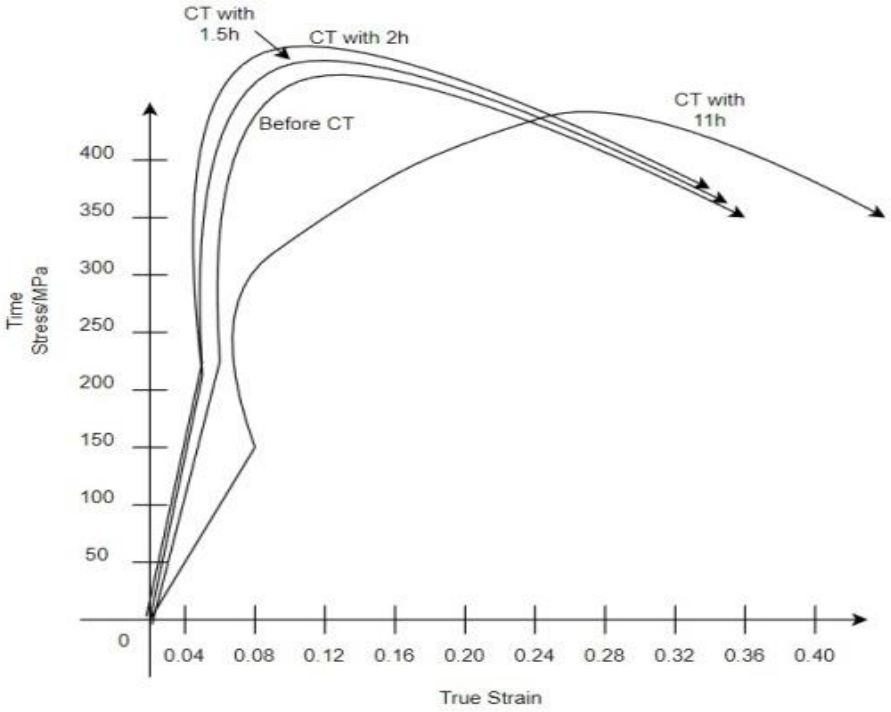

Fig 4. Stress-Strain curve of Mg mixture AZ-91 in Cryogenic Test.

Cryogenic treatment is a powerful technique that can specifically enhance the total mechanical characteristics of magnesium alloys. This treatment of mg mixture will result in condense of the amethyst fretwork, which is undoubtedly advantageous for refining grains and changing texture. However, it will also hasten the precipitation of the 2nd period and the peer group of disruption, which can significantly enhance the metal properties. In addition, twins appeared during the cryogenic rolling of magnesium alloys. Due to the anomalous activation of pyramidal disruption, the WE43 alloy experienced an increase in strength and elongation under cryogenic compression [16]. The maximum tensile strength and extensibility of something like the Magnesium-14Lithium-1Aluminiummixture with cryogenic rotation were enhanced by 50% (227 MPa) and 4 times (29.8%), respectively, thanks to Dynamic phase transformation and micro shown in **Table 3**. The investigation on this behaviour towards of AZ91 mixture, however, is very new and there aren't as many reports as there are on this test of material. This is especially true for this treatment of Mg alloys after hot spinning. As a result, the work on the cryogenic test of Mg composite after hot spinning has some theoretical as well as practical value shown in **Table 4**.

Table 1. The chemical composition of AZ91 Magnesium Alloy

						Wt%
Al	Zn	Mn	Fe	Cu	Ca	Mg
8.31	0.76	0.21	0.017	0.06	0.012	Bal.

Table 2. Mechanical properties of the specimen (Cryogenic Test)

Cryogenic time/h	Peak stress/MPa	True strain
0	213.4	0.1
1	235.7	0.12
3	246.7	0.13
5	244.5	0.15
10	241.3	0.24
24	254.2	0.25

Table 3. The Constant in a single-arm direct current electric bridge circuit

Electric resistance	Before CT	After CT
R1/Ω	97	97
R2/Ω	97	10 223
K	3	10^-3

Table 4. Electric resistance (Cryogenic Treatment for samples)

Cryogenic time/h	Before CT /Ω	After CT/Ω
2	4.87	0.116
8	4.87	0.114
23	4.87	0.113

VI. FATIGUE FRACTURE TEST

Experiments on the development of fatigue cracks were carried out using the high strength magnesium alloy AZ91. According to T351, the material underwent heat treatment that included solution strengthening, extinguish, metal without the usage of heat, and age solidify. The material has a norm grain size of 200 m while rolling in the L direction, 75 min when rolling in the T direction, and 40 min when rolling in the S direction in the whole metal piece. The work piece was oriented equidistant to the direction of rolling. The 2024-T351 was used for research on ultrasonic durability with random and constant amplitude loading. A constant blow-by of ambient air was used to continuously infuse distilled water (20–22°C) with oxygen for constant amplitude studies [17]. Using a normal distribution of cargo, a computer control adjusts the magnitude of subsequent pulses in random amplitude testing. This indicates that a Rayleigh distribution characterises the load amplitude distribution. The pulse sequence, which had a length of 1 million, was produced using a Markov distribution. The use of ultrasonic frequency equipment to replicate in-service loading is described in further detail elsewhere. Utilizing computer control, all cargo rotation applied to the work piece are assessed. Damage buildup is carried out using the actual measured load amplitudes [18].

The development of fatigue cracks properties of a uniform grid notches workpiece with a depth of 4 millimeters and a width of 17 mm were researched at a frequency range in surroundings vent, shrivelled aspect, and a vacuity and the results are attached in the **Fig 5**. Chilling airflow to the freezing of liquid nitrogen generated dry air. Unfortunately, the precise relative humidity could not be determined. Break mature outlay were computed in 4-9% of the genuine rotation pressure potency worth using a typical load-shedding technique. The break mature outlay was calculated using break length gain of around 1.20- 1.30 millimeter. During pulse-pause loading, the fracture length was measured at the workpiece faces using an in-situ video camera. The optical system had a magnification of 180. Mechanics of ultrasound endurance and tension fissure progression tests, periodic strain energy computation, and data validation are discussed in full here.

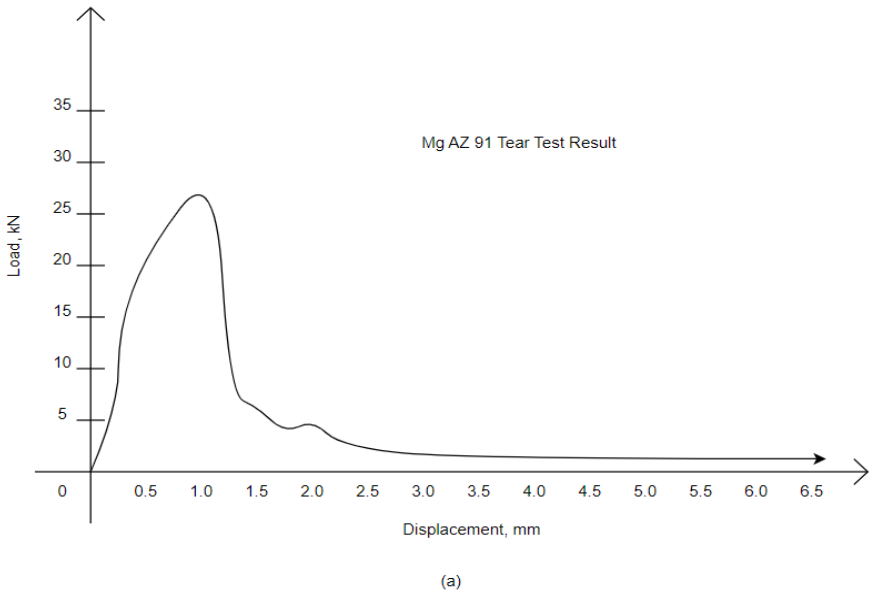

Fig 5. Load Displacement Curve.

Failure flaws in workpieces 2024-T351 begin at the sample' surfaces in surrounding vent and sublime H2O. When distilled water is available, the SN curve shifts by 35-45% towards lower stress levels. Water is obviously toxic and severely reduces fatigue life. When the specimen was subjected to water for less than a moment, abrasive wear was already reduced for failure rates as low as 100. A (dashed) line less than 107 cycles can reasonably well mimic the SN curve shown in **Table 5**. Nonetheless, two workpieces did not break after more than 2 109 cycles at 70 MPa. The measured duration limit in water cannot be attributed to an "intrinsic yield point" or to the oxide coating safeguarding the aspect from more milieu mortification.

Table 5. Information of workpiece sample and test

Information of workpiece sample and test in this Fatigue Studies		
Metal	**Number of workpiece**	**Stress amplitude (Mpa)**
AZ91	2	65.8, 77.9, 83.2, 96.6, 107.9 and 113.6

VII. SEM ANALYSIS

Scanning Electron Microscopy is a method which will be used to identify the micro structure of the material, it will be scanned by the help of microscope. This will be mainly used to identify the micro level cracks present in the material while after the fatigue testing process. It will be work by the condition of a very high electron energies which will deliver by the work piece surface when it is revealed to a compressed concentrated electron rivulet from an electron rod. The space between the electron shooter and the work piece surface and the voltage accelerator can all be enhanced to accomplish the excellent possible pictures. In this SEM analysis there is a presence of two methods the first one is to identify various images of the sample piece of metal and the another one is the technique to analyse that one and all provide symbolic perspective. Depending on different types of chemical compositions in the whole image far field electrons can be identified to give dissimilarity. An atom provide an disparate x-rays they are unique to its atomic representation number when subjected to an electron beam, this shows the analysis of a representative primary structure, whether at a specific place or over a wide area, including line study and elemental portray. The chemical structure of a sample work piece metal can also be corrected by semi quantitative analysis. They also have the ability to analyse weight less components like nitrogen, O2 etc. Using WD X-rays [19]. when used in coincidence with quality scanning electron microscope (SEM) analysis, subatomic particle Dispersive X-rays can give a high level thorough explanation of the local part of a material. The most effective valued method is Electron Back Scattered Diffraction, which represents the microstructural pictures and identify the phase giving, strain, grain size and giving, and considered crystallo graphic inclination by using high level-intention crystallographic information. This used to be a rather specialised technique, but it may now be done frequently. Excellent sample preparation, which may be arranged through our metallography facilities, is crucial to the technique's success. With the use of scanning subatomic particle microscopes, we can resolve compositional and topographical images in incredibly fine detail at magnifications of 20–130,000. These pictures are generated by blitz a workpiece with concentrated subatomic particles, which produce a black and white picture from the subatomic particles that rebound the material. Electrons are detected using confidently imposed locator. Scanning subatomic particle microscopy, which employs variable pressure chambers, allows for 3D imaging of wet unit and substance as well as dried materials. Light microscopy is augmented by SEM photochemical analysis and internal imaging for the molecular profiling of prokaryotic organisms, crops, and primates. This section illustrates how to prepare workpiece for imaging that are moist, maintained, dry and non-conductive but covered with an electron conductive layer, and desiccated and conductive employing a Deben Cool stage in a hot and humid environment.

In an electrical resistance furnace, an AZ91 alloy melt was created in a steel crucible with adequate flux cover. When the melt temperature was around 750°C, charcoal particles with an average diameter of 21m were added. The melt was hand swirled for 60 seconds, allowing for optimum interaction between the ingredients. For 10 minutes, combine the melt and additions. It was then poured into warmed (350°C) cast iron cylindrical metallic moulds with a diameter of 25mm and a height of 125mm. Microstructural analysis was carried out on specimens made of 10mm dia. and 10mm height cut from these castings. To allow for grain size measurements, all microstructural workpiece were solution treated at 450 degree celsius for 24 hours before quenching in cold water. A mixture of 25% coke and 75% foundry sand bed was kept separate within the oven to absorb the atmosphere, limiting corrosion of Metal matrix composite samples during solution treatment. For microstructural investigation, the specimens were cleaned and scraped using an etchant (10 ml acetic acid, 15 ml water, 10 g picric acid, and 150 ml water solution). Leica DMRX optical microscope and JEOL, JSE 35C scanning electron microscopy (SEM) equipped with an energy dispersive spectrometer were used for the microstructural studies (EDS) [20]. The QWin image analysis programme was used to calculate the grain size. Using a powder diffractometer with Cu K radiation, a Phillips PW 1710, X-ray diffraction investigations were performed.

VIII. RESULTS AND DISCUSSION

Fatigue Fracture Test Result

When a tear test sample is subjected to static compressive stresses, a fracture starts at the source of the notch [21] and extends throughout the width of the specimen. The AZ91 study shows that a tearing test could provide two types of capacity curves [22]. The first, designated as "A," shows a large impulsive reduction in constant load after the peak point of load. In this situation, the breach starts at the point of greatest load. Some curves, known as item "B," indicate a consistent decrease in load after the yield stress, while fracture beginning occurs significantly before the yield stress. It has also been observed in samples with a thicknesses of less than 7 mm. Nevertheless, the only component of this investigation that causes this difference is the sample notch root radius value. It is roughly 22μ m in the situation A and m in 62μ m the case of B which is attached in **Table 6**. As a result, reducing the N reduction rate has a comparable effect to raising the thickness, resulting in the plane pressure state prevailing. It shows the main conclusions of tear tests on kind ″A″ and ″B″ samples in both Mg alloys as load-displacement curves and the results are attached in **Fig 6**.

The alloy's associated results such as having a powerful, point was taken, initiating efficiency (IE), and proliferation efficiency (PE) are presented for both tests. It can be shown that by applying different loads for two tests, the AZ91 alloy values increase, resulting in higher scratch strengths. This could be due to the alloy's higher precipitate content and, most likely, a broader precipitate free zone. The coarser particles and higher primary dry density of AZ91 explained the lesser 0.3 elastic modulus. Furthermore, regardless of specimen type, these curves show that AZ91 has a lower shatter induction efficiency (IE) than other materials.

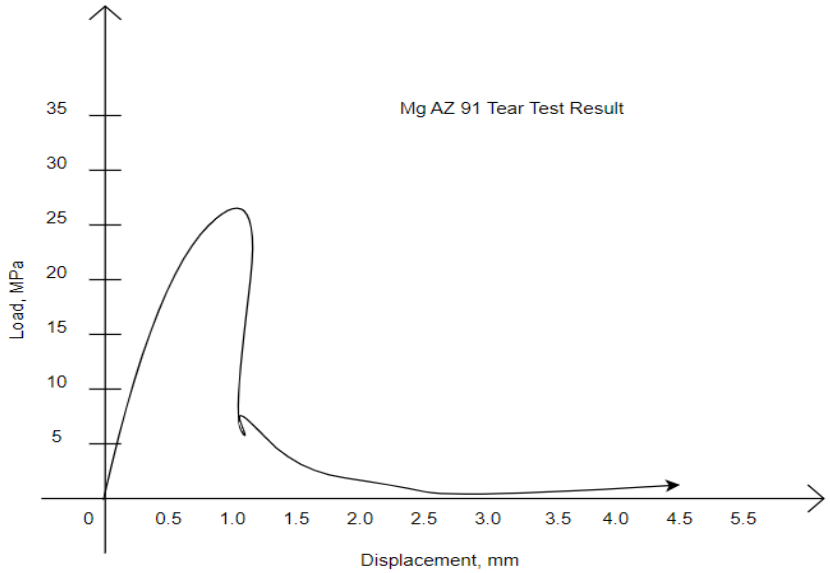

Fig 6. Fatigue Test Result.

Table 6. Fatigue Test Result

Alloy	Property							
	Specimen designation	NRR (μm)	Tear strength (MPa)	Notch 1 toughness	IE 2 (N.m)	PE 3 (N.m)	UIE 4 (kN/m)	UPE 5 (kN/m)
AZ91	A	22	627.21	2.12	25.30	7.75	153.56	51.76
AZ91	B	62	448.94	2.01	7.74	10.33	40.78	76.78

1. Tear strength divided by 0.2 (scratch toughness).
2. Energy for crack initiation.
3. The energy of crack propagation.
4. Combine initiation energy.
5. Propagation energy in units.

IX. CONCLUSION

The formation of a correct method solution increases peak pressure due to ordered strengthening. An ordered solid solution reduces electric resistance while simultaneously causing the crystallographic lattice constant to grow. CT transforms the as-cast AZ91 Mg alloy's structure from a disordered crystalline phase to an ordered cementite. CT could

promote second-phase particle precipitation and the formation of frame-type twinning. The enhanced second-phase phase particles are thought to be one of the key drivers of the ensuing deformation process's strengthening

The final conclusion can be drawn from the outcomes of this Fatigue Fracture Test investigation:

1. The tear test provides a variety of information, including notch toughness (the ratio of having a detrimental to yield strength), fracture initiating and dispersion energies, and notch diameters.
2. Intermetallic particles act as void generation and injury division sites, as well as initiation and propagation energies for unit cracks. The quantity, structure, and arrangement of intermetallic particles have been identified as significant parameters in the breakdown of the alloys being studied.
3. The alloy studied has the same damage beginning mechanism, however, the failure mechanism changes slightly. In a ripped specimen, collapse begins at the groove base in a flat trapezoidal zone transverse to the compression side.
4. In a ripped specimen, breaking begins at the hole base in a flat trapezoidal region as opposed to the compression side.
5. The alloy exhibits two significant failure segments and sub depending on the stress condition: ″internal smooching mechanism″ and ″void strip mechanism″.

Reference

[1]. X. C. Luo et al., “Enhancing mechanical properties of AZ61 magnesium alloy via friction stir processing: Effect of processing parameters,” Materials Science and Engineering: A, vol. 797, p. 139945, Oct. 2020, doi: 10.1016/j.msea.2020.139945.

[2]. H. Seifiyan, M. Heydarzadeh Sohi, M. Ansari, D. Ahmadkhaniha, and M. Saremi, “Influence of friction stir processing conditions on corrosion behavior of AZ31B magnesium alloy,” Journal of Magnesium and Alloys, vol. 7, no. 4, pp. 605–616, Dec. 2019, doi: 10.1016/j.jma.2019.11.004.

[3]. F. Muhaffel and H. Cimenoglu, “Development of corrosion and wear resistant micro-arc oxidation coating on a magnesium alloy,” Surface and Coatings Technology, vol. 357, pp. 822–832, Jan. 2019, doi: 10.1016/j.surfcoat.2018.10.089.

[4]. M. Asaduzzaman Chowdhury, MD. Helal Hossain, N. Hossain, Z. Hossen, Md. Arefin Kowser, and Md. Masud Rana, “Advances in coatings on Mg alloys and their anti-microbial activity for implant applications,” Arabian Journal of Chemistry, vol. 15, no. 11, p. 104214, Nov. 2022, doi: 10.1016/j.arabjc.2022.104214.

[5]. G. Ramesh, G. Gokilakrishnan, B. G. Jayaraja, and P. P. Patil, “High-content Al-T6/pineapple fiber/brass mesh reinforcements on nanosilica-toughened epoxy hybrid natural fiber metal laminate composite for aircraft applications,” Biomass Conversion and Biorefinery, Oct. 2022, doi: 10.1007/s13399-022-03354-8.

[6]. L. Chen, Y. Zhao, M. Li, L. Li, L. Hou, and H. Hou, “Reinforced AZ91D magnesium alloy with thixomolding process facilitated dispersion of graphene nanoplatelets and enhanced interfacial interactions,” Materials Science and Engineering: A, vol. 804, p. 140793, Feb. 2021, doi: 10.1016/j.msea.2021.140793.

[7]. M. Vigneshkumar, S. S. Murugan, P. A. Varthanan, G. Gokilakrishnan, N. Gobikrishnan, and A. P. Pagutharivu, “High velocity oxygen fuel coating for enhancing tribological behaviour of engineering metals,” AIP Conference Proceedings, 2022, doi: 10.1063/5.0108133.

[8]. X. Fu, K. Chen, C. Liu, M. Wang, and X. Hua, “Microstructure and mechanical properties of dissimilar friction stir lap welding between AZ31 Mg alloy and DC01 steel,” Materials Characterization, vol. 187, p. 111870, May 2022, doi: 10.1016/j.matchar.2022.111870.

[9]. P. Satishkumar, G. Gokila Krishnan, S. Seenivasan, and P. Rajarathnam, “A study on tribological evaluation of hybrid aluminium metal matrix for thermal application,” Materials Today: Proceedings, vol. 81, pp. 1097–1104, 2023, doi: 10.1016/j.matpr.2021.04.389.

[10]. E. Khalid, V. C. Shunmugasamy, and B. Mansoor, “Microstructure and tensile behavior of a Bobbin friction stir welded magnesium alloy,” Materials Science and Engineering: A, vol. 840, p. 142861, Apr. 2022, doi: 10.1016/j.msea.2022.142861.

[11]. G. Gokilakrishnan et al., “Wear Behavior and FESEM Analysis of LM 25 Alloy MMHCs Reinforced with FE3O4 and Gr by Utilizing Taguchi’s Technique,” Journal of Nanomaterials, vol. 2022, pp. 1–10, Jul. 2022, doi: 10.1155/2022/3203057.

[12]. J. Liang et al., “Microstructure evolution of laser powder bed fusion ZK60 Mg alloy after different heat treatment,” Journal of Alloys and Compounds, vol. 898, p. 163046, Mar. 2022, doi: 10.1016/j.jallcom.2021.163046.

[13]. J. Rong et al., “A high performance Mg–Al–Ca alloy processed by high pressure die casting: Microstructure, mechanical properties and thermal conductivity,” Materials Science and Engineering: A, vol. 849, p. 143500, Aug. 2022, doi: 10.1016/j.msea.2022.143500.

[14]. J. Gao, Y. Su, and Y.-X. Qin, “Calcium phosphate coatings enhance biocompatibility and degradation resistance of magnesium alloy: Correlating in vitro and in vivo studies,” Bioactive Materials, vol. 6, no. 5, pp. 1223–1229, May 2021, doi: 10.1016/j.bioactmat.2020.10.024.

[15]. X. Yang et al., “Hot tensile deformation behaviors and a fracture damage model of the Mg-Gd-Y-Zn-Zr alloy,” Journal of Materials Research and Technology, vol. 18, pp. 255–267, May 2022, doi: 10.1016/j.jmrt.2022.02.104.

[16]. M. Esmaily et al., “A detailed microstructural and corrosion analysis of magnesium alloy WE43 manufactured by selective laser melting,” Additive Manufacturing, vol. 35, p. 101321, Oct. 2020, doi: 10.1016/j.addma.2020.101321.

[17]. S. Tang et al., “Precipitation strengthening in an ultralight magnesium alloy,” Nature Communications, vol. 10, no. 1, Mar. 2019, doi: 10.1038/s41467-019-08954-z.

[18]. J. X. Wei, H. Yan, and R. S. Chen, “Notch strength and notch fracture mechanisms of a cast Mg-Gd-Y alloy,” Materials Science and Engineering: A, vol. 835, p. 142668, Feb. 2022, doi: 10.1016/j.msea.2022.142668.

[19]. R. Viswanathan, S. Ramesh, S. Maniraj, and V. Subburam, “Measurement and multi-response optimization of turning parameters for magnesium alloy using hybrid combination of Taguchi-GRA-PCA technique,” Measurement, vol. 159, p. 107800, Jul. 2020, doi: 10.1016/j.measurement.2020.107800.

[20]. J. Wu, L. Jin, J. Dong, F. Wang, and S. Dong, “The texture and its optimization in magnesium alloy,” Journal of Materials Science & Technology, vol. 42, pp. 175–189, Apr. 2020, doi: 10.1016/j.jmst.2019.10.010.

[21]. D. Saravanan, G. Gokilakrishnan, and C. R. Raajeshkrishna, “Effect of carbon/kevlar reinforcement and hybrid order on mechanical properties of glass/epoxy composites,” Advances in Materials and Processing Technologies, vol. 8, no. 3, pp. 3377–3388, Aug. 2021, doi: 10.1080/2374068x.2021.1965719.

[22]. V. Murugesan, P. A. Varthanan, S. S. Murugan, and G. Gokilakrishnan, “NUMERICAL ANALYSIS OF THE EFFECT OF HEAT INPUT IN THE SPOT WELDING OF DISSIMILAR MATERIALS,” Materiali in tehnologije, vol. 56, no. 3, Jun. 2022, doi: 10.17222/mit.2022.411.